Biointerface Research in Applied Chemistry
Open-Access Journal (ISSN: 2069-5837)

Article
Volume 16, Issue 1, 2026, 6
https://doi.org/10.33263/BRIAC161.006

Determination of Creatinine as Kidney Function Biomarkers using Immobilised Biogenic Silver Nanoparticles on a Microfluidic Paper-Based Analysis Device (µPAD)

Dhony Hermanto [1,*], Yustika Yustika [1], Lely Kurniawati [1], Ulul Khairi Zuryati [2], Bambang Kuswandi [3], Nurul Ismillayli [1]

[1] Department of Chemistry, Faculty of Mathematics and Natural Sciences, University of Mataram, Mataram–West Nusa Tenggara 83125, Indonesia
[2] Laboratory of Analytical Chemistry, University of Mataram, Mataram–West Nusa Tenggara 83125, Indonesia
[3] Chemo and Biosensor Group, Faculty of Pharmacy, University of Jember, Jember– East Java 68121, Indonesia
* Correspondence: dhony.hermanto@unram.ac.id;

Received: 3.11.2025; Accepted: 21.01.2026; Published: 15.02.2026

Abstract: Early identification of kidney failure is crucial since it can advance silently without noticeable symptoms. Measuring creatinine, a waste product filtered by the kidneys, is an effective early diagnostic tool to prevent progression, reduce healthcare costs, and delay severe complications such as cardiovascular disease and anemia. In this study, a paper-based microfluidic sensor utilizing biogenic silver nanoparticles (AgNPs) was developed for the colorimetric detection of creatinine. AgNPs were electrochemically synthesised with Orthosiphon aristatus extract (OAE) containing flavonoids (1.71±0.16 mg/g) and phenols (23.79±1.48 mg/g) as an electrolyte and stabilising agent to produce spherical AgNPs with a size of approximately 17.44±3.68 nm. The AgNPs were then immobilised on microfluidic paper to serve as a colorimetric creatinine detector. The sensor response was evaluated using RGB (Red, Green, Blue) analysis, which compared the colour intensity before and after interaction with creatinine. The addition of creatinine replaced the OAE-derived biomolecular capping layer on the AgNP surface, confirming the ligand exchange mechanism that induces some particles might undergo agglomeration, allowing the formation of larger nanoparticles (17.44±3.68 nm to 21.09±5.92 nm) while maintaining the fcc silver crystal structure as indicated by FTIR, SEM-EDX, PSA, XRD, and TEM measurements. The developed sensor exhibited a linear range of 1–100 µg/L, with a limit of detection (LOD) of 1.6 µg/L, confirming excellent sensitivity for the early detection of kidney disease. Furthermore, the optical readout demonstrated high precision, with intra-day and inter-day relative standard deviation (RSD) values of below 4% and 6%, respectively. Even in the presence of potential interferents at tenfold higher concentrations, the sensor maintained remarkable selectivity. Application in artificial urine yielded satisfactory recovery (R) rates (96.3–102.6%), confirming that AgNP@OAE paper-based microfluidic sensor is a simple, cost-effective, and reliable tool for point-of-care creatinine monitoring and early renal diagnostics.

Keywords: biogenic AgNP; creatinine; kidney function biomarkers; microfluidic paper; RGB analysis.

© 2026 by the authors. This article is an open-access article distributed under the terms and conditions of the Creative Commons Attribution (CC BY) license (https://creativecommons.org/licenses/by/4.0/), which permits unrestricted use, distribution, and reproduction in any medium, provided the original work is properly cited. The authors retain copyright of their work, and no permission is required from the authors or the publisher to reuse or distribute this article, as long as proper attribution is given to the original source.

1. Introduction

Creatinine, the end product of creatine metabolism, is primarily excreted by the kidneys as a vital blood-filtering organ [1]. Its concentration in serum and urine is a key physiological indicator for diagnosing kidney disorders and monitoring kidney function, with 15–20% of cases progressing to chronic kidney disease (CKD) within two years [2,3]. Early diagnosis and timely intervention can prevent or delay the progression of CKD [4]. Despite this, kidney failure is often misdiagnosed and undertreated in its early stages, in part due to the lack of an established classification system and readily accessible and cost-effective detection tools. Consequently, the development of rapid and reliable diagnostic tools is critical for determining the initial disease status and preventing further progression [5].

A variety of analytical approaches—including chromatography, electrochemistry, capillary electrophoresis, liquid chromatography-isotope dilution mass spectrometry (LC–IDMS) [6], paper-spray ionization-mass spectrometry (PSI-MS) [7], and Raman or surface-enhanced Raman spectroscopy (SERS) [8]– have been employed for creatinine quantification in biological fluids. Although highly accurate, these methods are limited by labor-intensive sample preparation, reliance on hazardous reagents, the need for expensive and sophisticated instrumentation, and the requirement for skilled operators. As such, they are impractical for routine, high-throughput, real-time analysis in clinical laboratories [9]. The Jaffé reaction, a classical colorimetric assay based on the formation of a creatinine–picric acid complex in alkaline conditions, has been widely adopted as an alternative [10]. However, its clinical value is limited by interference from endogenous metabolites and medications, which diminish assay specificity. Pseudochromogen interference, such as plasma proteins, caused a 0.3 mg/dL (27 µmol/L) rise in creatinine levels [11]. Furthermore, picric acid's caustic and explosive properties limit its application. These challenges highlight the urgent need for a rapid, simple, low-cost, sensitive, and selective method for direct creatinine detection in biological specimens.

In this context, AgNP-based colorimetric sensors have emerged as promising candidates due to their unique optical properties, which depend on particle size, morphology, composition, and localized surface plasmon resonance (LSPR) [12]. The visible LSPR absorption of AgNPs allows straightforward colorimetric detection [13,14], as the resulting color changes can be visually observed without advanced instrumentation [15]. AgNPs have been successfully applied as colorimetric probes for various analytes [16,17], including creatinine [18]. For instance, Alula et al. [19] developed citrate-stabilized AgNPs as colorimetric and spectrophotometric probes for creatinine in human urine, and other studies have employed 2,2′-thiodiacetic acid (TDA)-modified AgNPs to measure creatinine in human serum, plasma, and urine fluid [20]. Glassy carbon electrodes (GCE) designed in the form of nanocomposites AgNPs at titanium dioxide (TiO_2)/graphene oxide (GO) nanocomposites (Ag@GO/TiO_2-GCE), were also used to detect creatinine electrochemically [21]. Despite these advancements, existing techniques still have constraints, such as the need for sophisticated nanoparticle functionalization, lengthy sample preparation, and high manufacturing costs, which limit their use in fast, real-time applications. To address these problems, the current study suggests a simple, quick, and affordable colorimetric probe based on plant extract-mediated (biogenic) AgNPs. In addition, combining biomolecules with electrolysis methods in biogenic AgNP synthesis enables the formation of nanoscale, uniform particles, thereby improving their performance as sensing agents for analyte detection [14]. The use of

Orthosiphon aristatus leaf extract (OAE) in biogenic AgNP synthesis is a sustainable, environmentally friendly technology that reduces the use of hazardous chemicals. Previous studies have shown that OAE includes hydroxyl group-rich flavonoids, rosmarinic acid, and polyphenolics [22], which serve as excellent stabilisers and bioreductants. The presence of biomolecules on the AgNP surface enables it to interact with creatinine and induce specific changes in the LSPR, thereby enabling selective detection and measurement of creatinine.

2. Materials and Methods

2.1. Materials.

Creatinine used for the preparation of standard solutions was obtained from Sigma-Aldrich (USA). A commercial creatinine colorimetric kit, employed for comparative analysis, was sourced from Glory Diagnostics (Spain). Biogenic AgNPs were synthesized via green electrosynthesis using two silver rod electrodes (Antam, Indonesia) and Orthosiphon aristatus extract (OAE) as the electrolyte. All other reagents were of analytical grade and purchased from Sigma-Aldrich (USA). Double-distilled water (oneMed, Indonesia) and buffer solutions (Merck, UK) were used for solution preparation.

2.2. Preparation of OAE and phytochemical content.

OAE is prepared by air-drying OA leaves and macerating them with distilled water at a 1:10 ratio overnight. The total phenolic content (TPC) of OAE was quantified using the Folin–Ciocalteu method. In brief, 1 mL of OAE (12.5 mg/mL) was mixed with 50 µL of 50% Folin-Ciocalteu reagent and 2 mL of 2% sodium carbonate (Na_2CO_3) solution. The mixture was completely homogenized and incubated for 30 minutes. The total flavonoid content (TFC) was assessed using the aluminum chloride ($AlCl_3$) colorimetric method, forming a flavonoid-aluminum complex. In this assay, 1 mL of OAE (12.5 mg/mL) was mixed with 1 mL of 2% methanolic $AlCl_3$ solution. The mixture was thoroughly homogenized and incubated for 15 min. Absorbance was subsequently recorded at 720 nm (TPC) and 415 nm (TFC) using a UV–Vis spectrophotometer (UV-7809, Labo-Hub, China) [23]. A calibration curve was generated using rutin standards (1.00–35.00 mg/L for TPC and TFC), and TPC/TFC was expressed as mg of rutin equivalent (RE) per g of dry extract weight. All measurements were performed in triplicate unless stated otherwise.

2.3. Preparation and characterization of biogenic AgNPs.

Biogenic AgNPs were synthesized using a green electrosynthesis process as previously reported by Hermanto et al. [23,24]. The OAE solution is used as an electrolyte as well as a bioreductant and capping agent, with the original pH of the solution without adjustment (~5.5). Two silver rod electrodes 0.5 cm apart were immersed in the OAE electrolyte and connected to a 0.1 mA and 10 V direct current (DC) power supply at room temperature (~ 28°C), with polarity alternated every minute using a control switch. A color change of the solution from greenish-yellow to brownish-yellow was observed visually after 3 minutes of electrosynthesis, confirming the formation of AgNPs. The nanoparticles were purified by centrifugation at 12,000 rpm (MDX 310, Tomy, Japan), followed by freeze-drying (Alpha 1-2LDplus, Germany, equipped with an RZ 2.5 vacuum pump). The dried biogenic AgNPs were re-dispersed in

double-distilled water to obtain colloidal biogenic AgNPs, which were subsequently used as biosensing indicators for further analysis.

Multiple analytical techniques were employed to characterize the biogenic AgNPs produced in the previous step. Biogenic AgNPs exposed to creatinine were also characterized. The LSPR of the AgNPs was determined using a UV–Vis spectrophotometer (UV 7809, Labo-Hub, China). The existence of functional groups responsible for biomolecular interactions during AgNP production was investigated using Fourier transform infrared spectroscopy (FTIR; PerkinElmer, USA). The sample powder and potassium bromide (KBr) powder were blended and pressed at 700 kN for 3 min to form a pellet shape. The FTIR measurements were taken at room temperature and ranged from 4000-400 cm^{-1}. Scanning Electron Microscopy (SEM; JEOL-JEM, Japan) at 15,000 kV and ×3,000 magnification and Transmission Electron Microscopy (TEM; Hitachi H9500, Japan) at room temperature with an acceleration voltage of 120 kV and ×100,000 magnification were used to visualize morphological aspects, such as particle form and size distribution. X-ray diffraction (XRD; Philips X'pert PW3050, Netherlands) was also used to examine the crystalline phase, shape, and average crystallite size. The measurement settings include continuous scanning at 2 theta 5 - 90°, a scan step length of 10.1500 s, a generator setting of 30 mA and 40 kV, and a temperature of -273.15°C. The anode material is Cu with K-alpha 1.54 Å. The crystallite size (D) was determined using the Debye-Scherrer equation, $D=k\lambda/\beta\cos$, where k represents the shape factor (0.94), λ is the X-ray wavelength, β is the full width at half maximum (FWHM), and θ is the Bragg diffraction angle. The size distribution (size and polydispersity index, PDI) of AgNPs was analyzed using a Malvern Zetasizer (PSA; Malvern Instrument, UK) with water as solvent dispersant, measurement temperature at 25 °C, duration 60 s, and count rate 299.2 kcps.

2.4. Fabrication of the colorimetric probe.

Whatman No. 42 filter paper (2.5 µm pore size) served as the solid support and colorimetric probe medium for the microfluidic device [15]. Paper probes (1 cm^2) were soaked overnight in a 1% PVA solution containing 10 µL of colloidal biogenic AgNPs (10 µg/mL), allowing efficient AgNP immobilization on cellulose fibers. Following the immobilization, the paper was air-dried overnight in a chiller at 10°C until the hue changed from white to yellow. The AgNP-embedded microfluidic papers were refrigerated until use. These probe-modified papers were produced in different fabrication runs under identical conditions. The reproducibility, surface uniformity, and paper-to-paper variation of the colorimetric probe paper were assessed using the coefficient of variation (CV). Colorimetric responses were quantified and reported as CV following exposure to a reference analyte concentration; values less than 10% were considered acceptable.

2.5. Operation procedure µPADs.

Microfluidic paper-based analytical devices (µPADs) were used as colorimetric sensors to detect creatinine via visible color changes. Colorimetric responses were examined using RGB values. To ensure consistent illumination and temperature settings, images were taken inside a custom-built photo box (75 × 50 × 50 cm^3) with LED lighting, 5500 K, ISO 100, exposure 1/60 s, white balance manual paper (references), and a camera distance of 15 cm. Images were captured with a 50 MP smartphone camera (Techno Spark 20C, which has a MediaTek Helio G36 chipset that supports smooth camera performance and quick image

processing with JPEG format; Techno Mobile-Transition Holdings, Shenzhen, China) and processed with ImageJ software to extract RGB values from the reactive zones. A calibration curve was constructed by plotting RGB intensity values against known concentrations of standard solutions. Creatinine standard solutions (1–100 µg/L) were freshly prepared by diluting the stock solution with Tris-HCl buffer (pH 7.2). For long-term storage, aliquots of the stock solution were stored at −20°C to maintain stability. Creatinine concentrations in test samples were then determined by fitting the sample RGB values into the linear regression equation derived from the calibration graph.

2.6. Creatinine detection.

The AgNP@OAE-based microfluidic paper was measured for creatinine concentrations ranging from 1 to 100 µg/L, resulting in a mean RGB-concentration plot. The color was shifted from brownish yellow to pale yellow. The selectivity was evaluated by replacing creatinine with potential interferents (citrate, glucose, ascorbic acid, urea, and uric acid) and recording the corresponding AgNP@OAE-based microfluidic paper values. Artificial urine was prepared following a reported protocol by dissolving urea, uric acid, potassium chloride (KCl), sodium chloride (NaCl), calcium chloride ($CaCl_2$), tri-sodium citrate dihydrate ($Na_3C_6H_5O_7 \cdot 2H_2O$), ammonium chloride ($NH_4Cl$), potassium oxalate heptahydrate ($K_2C_2O_4 \cdot 7H_2O$), sodium di-hydrogen phosphate dihydrate ($NaH_2PO_4 \cdot 2H_2O$), and di-sodium hydrogen phosphate dihydrate ($Na_2HPO_4 \cdot 2H_2O$) in 100 mL of double-distilled water using a magnetic stirrer at room temperature [25]. The samples were diluted with phosphate buffer (1:20), spiked with defined concentrations of creatinine, and used for actual sample analysis.

3. Results and Discussion

In this work, a comprehensive approach was employed to develop a creatinine-sensing platform based on biogenic AgNPs. The methodology involved three sequential steps: (i) electrochemical synthesis of AgNPs using OAE as a green electrolyte, (ii) physical immobilization of the obtained nanoparticles onto cellulose filter paper, and (iii) application of the functionalized paper in a colorimetric sensing scheme for creatinine detection (Figure 1). This integrated process offers a sustainable route for nanoparticle production and sensor fabrication while minimizing the use of toxic chemicals. The combination of electrochemical, physical, and chemical steps yielded a low-cost, portable sensing system with potential for point-of-care diagnostics.

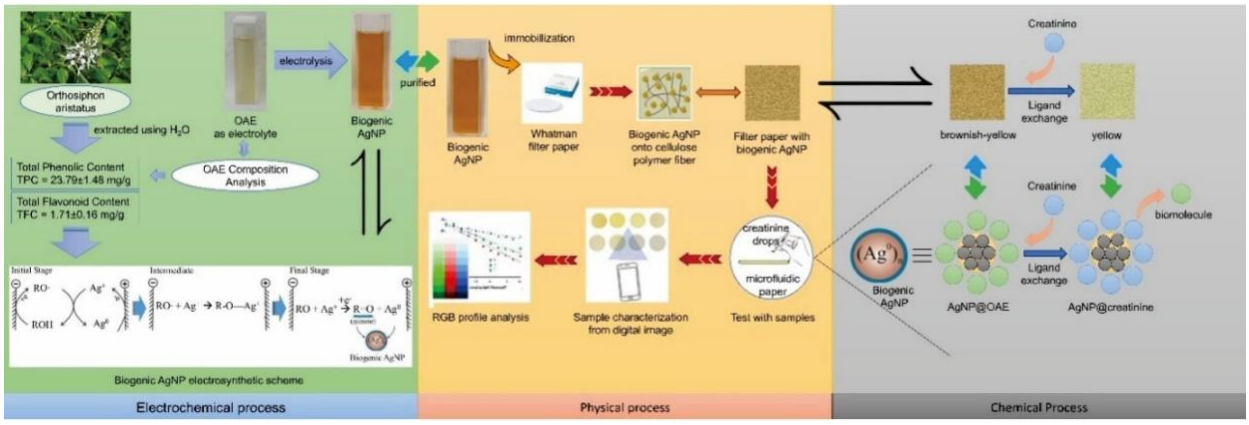

Figure 1. A comprehensive approach in preparing biogenic AgNP, sensor fabrication, and its mechanism in detecting creatinine.

According to Figure 1, the biosynthesis of AgNPs was carried out using electrolysis with two silver electrodes serving as anode and cathode immersed in OAE solution. During the procedure, Ag^+ ions were liberated from the anode and reduced in situ by phytochemicals in the extract. Phenolic and flavonoid contents serve as bioreductants, allowing controlled nucleation and development of AgNPs while also providing capping activity to improve colloidal stability. This single-step electrochemical approach avoided the need for synthetic reducing chemicals and produced uniformly dispersed nanoparticles suitable for further immobilization.

Figure 1 shows that OAE contains significant concentrations of ROH-containing chemical compounds, including flavonoids (1.71±0.16 mg/g, with the equation $y=0.016x+0.052$, $R^2=0.9866$, blank correction = 0.02) and phenols (23.79±1.48 mg/g, with the equation $y=0.0325x+0.1854$, $R^2=0.9883$, blank correction = 0.08), indicating its ability as a bioelectrolyte for the electrosynthesis of biogenic AgNPs. Applying a 10 V DC potential in the electrolytic reactor promoted silver anode oxidation, resulting in Ag^+ ions [26]. The biomolecules in OAE (R-OH) are reduced to produce RO· radicals and release electrons when a direct current voltage source is applied. Then, these radicals formed R-O-Ag^+ complexes, inhibiting cathodic deposition and promoting nanoparticle nucleation [27,28]. Continuous stirring at 2000 rpm under ambient conditions facilitated complex formation, allowing for Ag^+ reduction to Ag^0 by the -OH group on the OAE biomolecule. This was subsequently oxidised to quinone (R=O) and contributed to biomolecule-assisted capping and stabilisation of the AgNP surface [24,28,29]. Reversing the electrode polarity once every minute reduces anode depletion and inhibits water electrolysis, preventing silver oxide accumulation that could hinder current flow [23]. Overall, this electrochemical route offers a rapid, scalable, and cost-effective strategy for synthesizing high-purity AgNPs without employing toxic reagents.

The biogenic AgNPs were immobilized on Whatman filter paper via a physical adsorption (physisorption) process (Figure 1). Hydrogen bonds between the hydroxyl groups of cellulose fibers and the biomolecular layer covering the nanoparticles enabled the contact [15,30]. This non-covalent attachment ensured that AgNPs were uniformly distributed on the paper substrate, with no significant aggregation or loss of optical activity. The immobilized paper had a characteristic brownish-yellow color, confirming the successful attachment of AgNPs and the development of a functional sensing surface.

The immobilization of biogenic AgNPs onto cellulose-based filter paper results in a stable and uniformly distributed nanocomposite in which the nanoparticles are anchored by a combination of physical adsorption, hydrogen bonding, and weak biogenic AgNP (R=O---Ag) coordination with the hydroxyl groups of cellulose fibers [15,30]. This contact not only inhibits AgNP aggregation but also preserves their high surface-to-volume ratio, thereby maintaining their characteristics. Immobilized devices have been widely used as cost-effective and portable sensing platforms. The porous structure of the paper allows for rapid capillary-driven sample transport, resulting in efficient interaction between the analyte and the nanoparticle [31]. Meanwhile, the LSPR of AgNPs enables sensitive optical sensing, manifested as observable color changes or detectable spectral shifts upon analyte interaction. Effective immobilization minimizes nanoparticle leaching, thereby improving detection repeatability and reliability. As a result, AgNP-functionalized filter paper serves as both a passive filtration medium and an active sensing substrate, with potential applications broadened from environmental monitoring to diagnostics.

Figure 1 shows that the sensing mechanism was based on ligand-exchange interactions between creatinine molecules and surface-bound biogenic capping agents on AgNPs. Once creatinine was introduced to the microfluidic paper device, the hue changed from brownish-yellow to yellow, indicating a change in the LSPR of AgNPs. This colorimetric reaction can be detected by digital image analysis or spectrophotometry, enabling semi-quantitative or quantitative creatinine detection. The developed system thus provided a simple, reagentless, and cost-effective platform for creatinine monitoring in clinical and point-of-care settings.

The distinctive color of biogenic AgNPs is due to LSPR, a phenomenon arising from the interaction of incident electromagnetic radiation with the collective oscillation of conduction-band electrons on the nanoparticle surface. The physicochemical characteristics of nanoparticles, such as size, shape, spatial arrangement, and the surrounding medium's refractive index, significantly affect the location of the LSPR band. In the present study, the observed colorimetric reaction is due to AgNP aggregation, which is enhanced by creatinine's ligand-exchange and binding capabilities at the nanoparticle surface. As shown in Figure 2, the AgNPs are initially electrostatically stabilized by negatively charged biomolecule ligands, which create sufficient repulsive forces to prevent spontaneous aggregation. However, the biomolecule's carboxylate groups (quinone, R=O) have a relatively weak electrostatic contact with the nanoparticle surface, allowing displacement by ligands with higher binding affinities [32,33]. Creatine (which has an aromatic heterocyclic ring and three possible nitrogen coordination sites) rapidly adsorbs onto AgNPs by coordinating their nitrogen functional groups [34], substituting quinone. Creatine displaces quinone, yielding creatinine-functionalized AgNPs that promote nanoparticle aggregation and a visible shift in solution color. This ligand replacement has also been shown in a prior study [35]: adding creatinine to citrate-coated AgNPs can replace citrate ions, generating creatinine-coated AgNPs via Ag-N and Ag-π coordination interactions [33].

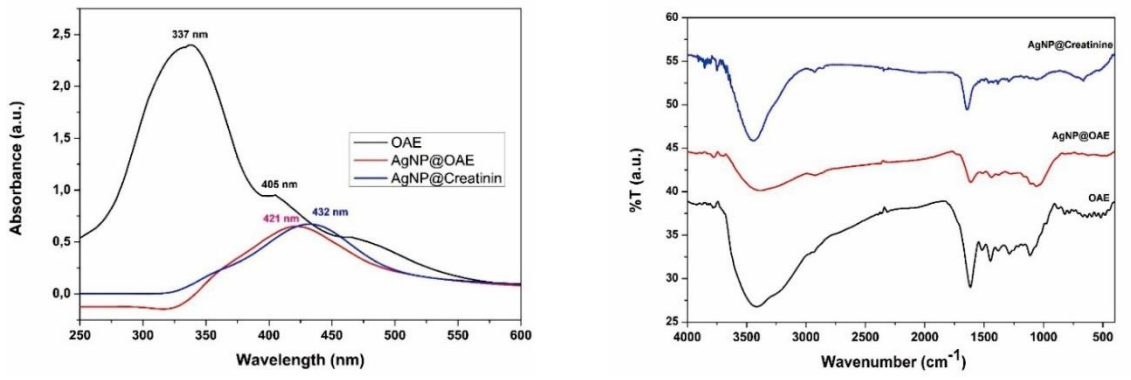

(a) **(b)**

Figure 2. (a) UV-Vis spectrum; **(b)** FTIR spectrum of OAE and AgNP@OAE before and after exposure to creatinine

The UV-Vis spectrum of the OAE extract exhibited a distinct absorption band at 337 nm (Figure 2a), which is attributed to the π–π* transitions of aromatic and conjugated biomolecules [36]. After the reduction of Ag^+ ions using OAE, a strong and well-defined LSPR peak emerged at 405 nm (Figure 2a) [24,37], confirming the formation of biogenic AgNP (AgNP@OAE). The narrow, symmetric SPR band indicates that the nanoparticles have a relatively uniform size distribution and remain well-dispersed in the medium. The disappearance of the original OAE peak and the emergence of the LSPR band collectively validate the successful biosynthesis of AgNPs through the bio-reductive action of OAE constituents.

Following exposure to creatinine, the LSPR band exhibited a redshift to 421–432 nm (Figure 2a) [35], accompanied by a slight broadening and increase in absorbance intensity. This red shift is consistent with a change in the local refractive index and indicates that some of the original OAE capping agent is replaced or rearranged by creatinine molecules. During ligand replacement, some particles may agglomerate, leading to the formation of larger nanoparticles, as confirmed by TEM and PSA analysis in the following discussion. Therefore, these spectral changes support the hypothesis of a surface-capping exchange process between OAE-derived molecules and creatinine on the AgNP surface [35].

Phytoconstituents of OAE, such as phenolic hydroxyls, carbonyls, and quinonoid moieties, donate electrons to convert Ag^{+} ions into metallic Ag^{0}, leading to the formation of AgNP@OAE. Based on Figure 2b, FTIR analysis of AgNP@OAE reveals a band at 1635 cm^{-1} corresponding to C=O stretching vibrations and a broad band around 3400 cm^{-1} suggesting O-H stretching. This confirms the participation of polyphenolic groups as both reducing and stabilizing agents. Peaks at 1384 cm^{-1} (C-O stretching) and 1050-1100 cm^{-1} (C-O-C or C-OH vibrations) confirm the nanoparticles' capping role. These molecules attach to the AgNP surface, inhibiting uncontrolled aggregation and ensuring colloidal stability.

Based on Figure 2b, FTIR spectrum of AgNP@Creatinine shows noticeable changes compared to AgNP@OAE, particularly the reduction in intensity of the quinone-associated C=O stretching at ~1635 cm^{-1} and the appearance of new features near 1550–1560 cm^{-1}, corresponding to N–H bending, as well as bands near 1300–1350 cm^{-1} attributed to C–N stretching of creatinine. These spectral shifts confirm a ligand exchange process, where quinone-based capping molecules are partially replaced by creatinine, leading to direct coordination between AgNP surfaces and creatinine's nitrogen atoms. This substitution alters the surface charge distribution, potentially enhancing the affinity of the nanoparticles for biomolecular interactions and modulating their physicochemical stability [35]. It was supported by EDS data as shown in Figure 3.

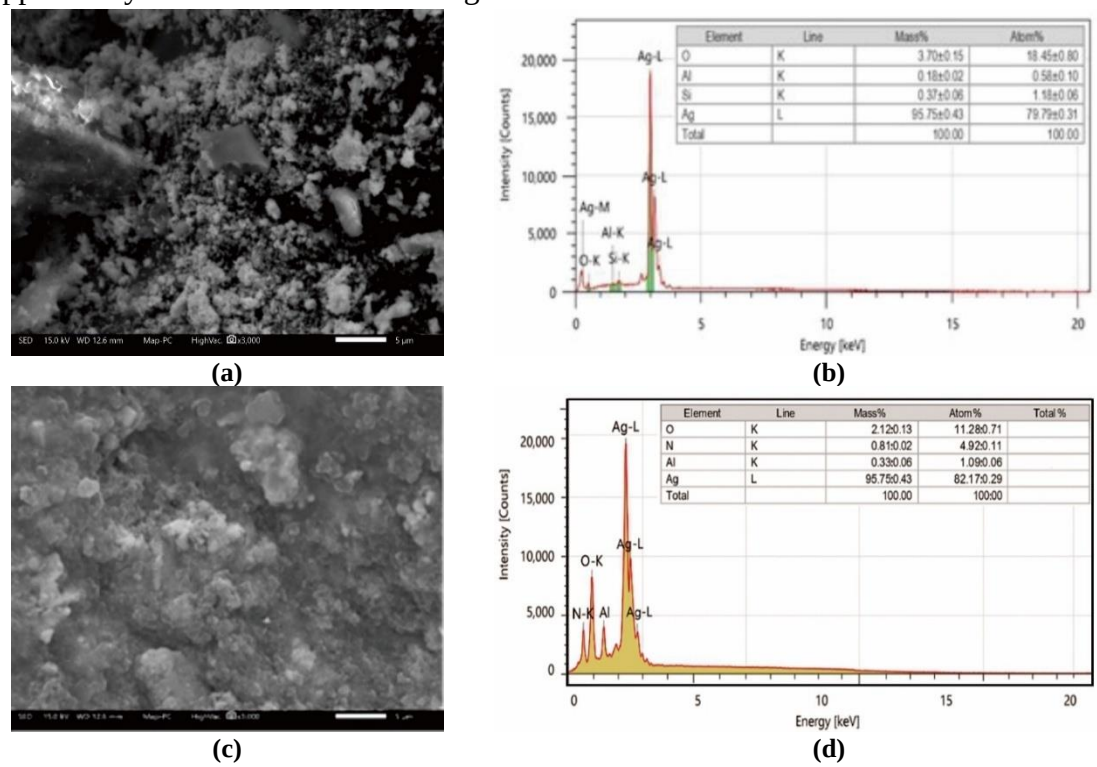

Figure 3. SEM images and EDS pattern of **(a,b)** AgNP@OAE; **(c,d)**AgNP@Creatinine.

The SEM micrograph of AgNP@OAE (Figure 3a) displays well-dispersed nanoparticles with only slight aggregation, suggesting that the OAE extract efficiently stabilises the silver nanoparticles and prevents agglomeration. The relatively uniform morphology supports the role of OAE as both a biogenic reducing agent and a capping agent, enabling the controlled synthesis of AgNPs. The EDS profile (Figure 3b) shows a dominant silver signal, accounting for nearly 95% of the total mass, accompanied by minor peaks from oxygen, aluminum, and silicon, likely derived from residual biomolecules and trace impurities in the synthesis medium. This is in line with previous research [23]; electrosynthesis using plant extracts produces AgNPs with high purity. The superior characteristics of biogenic AgNPs, such as high purity, uniformity of size and shape, and crystallinity, have a positive effect on the performance of the resulting sensor [14].

The SEM picture of AgNP@Creatinine (Figure 3c) shows a significant increase in aggregation, resulting in larger and denser clusters than AgNP@OAE. This morphological change suggests that ligand exchange between OAE and creatinine may reduce surface charge repulsion, promoting nanoparticle agglomeration, in line with a previous study [32]. The corresponding EDS spectrum (Figure 3d) shows a marked decrease in the oxygen peak and the emergence of nitrogen, confirming the replacement of OAE functional groups by creatinine on the nanoparticle surface [35]. During these surface alterations, the silver content remains roughly constant, suggesting that the nanoparticles' metallic core is maintained while their surface chemistry transforms, which could be useful for sensing applications. The clearer, more detailed shape and size distributions of AgNP@OAE and AgNP@Creatinine are shown in Figure 4.

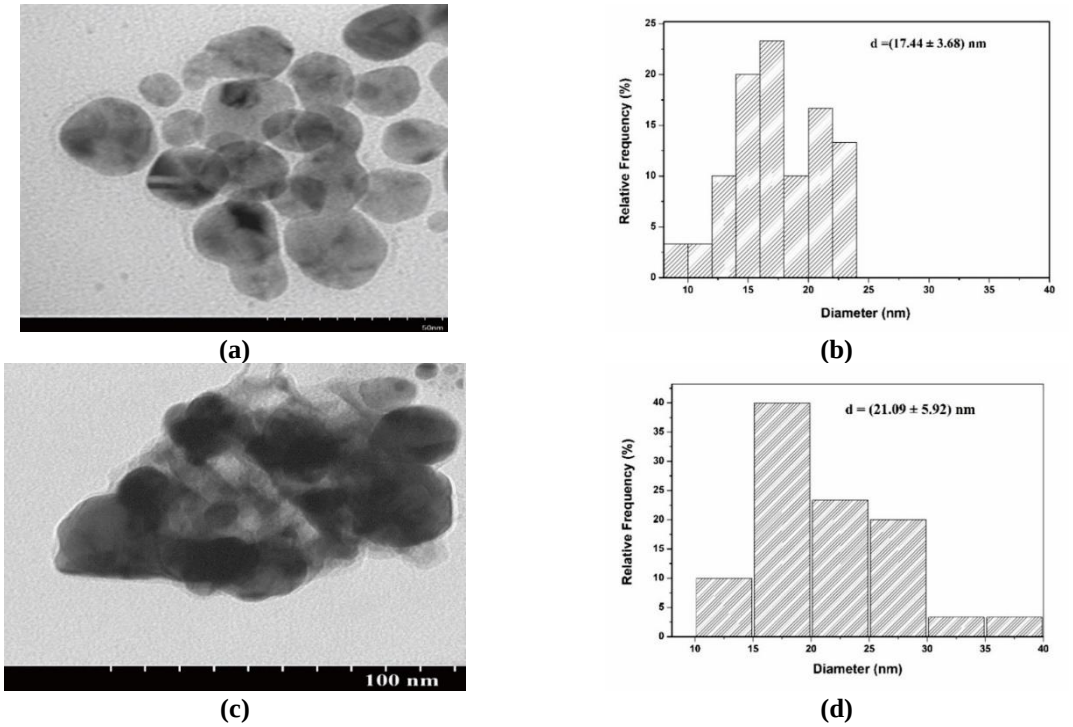

Figure 4. TEM images and particle size distribution of **(a,b)** AgNP@OAE; **(c,d)**AgNP@Creatinine.

The morphology, shape, and size distribution of AgNP@OAE were characterized using TEM. The AgNPs exhibited a relatively uniform spherical shape, as shown in the TEM images (Figure 4a). The particle size distribution was calculated, revealing an average diameter of 17.44 ± 3.68 nm (Figure 4b). The histogram indicates that most particles are concentrated in this size range, with minimal variation, highlighting the consistency of the synthesis process.

This suggests that the AgNPs are well-formed and maintain a stable size distribution, which is essential for their potential applications in various fields, such as biomedicine and catalysis.

The mechanism of ligand exchange on the surface of AgNP@OAE was investigated in the presence of creatinine. This interaction altered the shape and size distribution of the nanoparticles, leading to aggregation. The TEM images (Figure 4c) show that the AgNPs have undergone significant changes, transitioning from spherical nanoparticles to irregularly shaped clusters. The average particle size of AgNP@creatinine enlarged to 21.09 ± 5.92 nm (Figure 4d), due to aggregation caused by creatinine binding to the silver nanoparticle surface [32,35]. This aggregation process can alter the optical, chemical, and biological properties of AgNPs, reducing their performance in specific applications such as diagnostics. The changed shape and increased size distribution following creatinine exposure highlight the importance of ligand interactions in nanoparticle behavior. The increase in size is also shown by the PSA data in Figure 5.

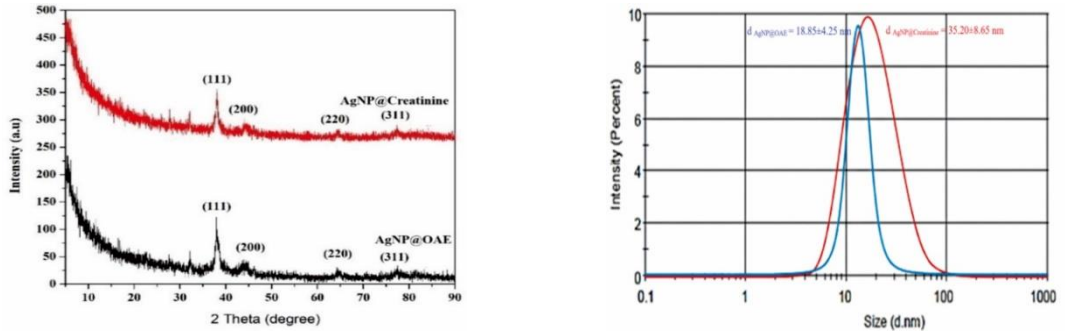

(a) **(b)**

Figure 5. (a) XRD pattern; **(b)** PSA profile of AgNP@OAE and AgNP@Creatinine.

XRD analysis revealed distinct diffraction peaks corresponding to the (111), (200), (220), and (311) planes, confirming the crystalline nature of the synthesized AgNPs (Figure 5a), consistent with previous reports [38,39]. The sample before creatinine exposure (AgNP@OAE) showed relatively sharp, intense peaks, indicating well-defined crystallinity. Upon exposure to creatinine, the diffraction pattern of AgNP@Creatinine exhibited a slight variation in peak intensity, suggesting minor structural modifications likely associated with ligand exchange on the nanoparticle surface. This change implies the successful replacement of the original capping agents with creatinine molecules, resulting in modified surface chemistry while maintaining the face-centered cubic (fcc) structure of silver nanoparticles.

PSA demonstrated that AgNP@OAE possessed an average hydrodynamic diameter of approximately 18.85 ± 4.25 nm, whereas AgNP@Creatinine showed an increased size of 35.20 ± 8.65 nm (Figure 5b). The broadening of the distribution after creatinine exposure suggests surface functionalization and possible partial aggregation, consistent with the ligand-exchange mechanism. These results indicate that creatinine molecules interact with the nanoparticle surface, leading to an increase in the overall hydrodynamic radius. Such a size enlargement [32] further supports the hypothesis of successful surface modification, which could influence the colloidal stability and reactivity of the nanoparticles in subsequent applications.

The selectivity of the AgNP@OAE sensing system was investigated by comparing its response to creatinine with those of various potential interferents, including citrate, glucose, ascorbic acid, urea, and uric acid (Figure 6a). At a concentration of 50 µg/L creatinine and 500 µg/L of the interferents, only creatinine induced a pronounced decrease in the mean RGB intensity, while the other tested molecules exhibited negligible effects. This finding demonstrates the superior selectivity of the sensing probe for creatinine, reducing the risk of

false-positive signals in complex biological samples. The selective recognition mechanism ensures that the system can reliably detect creatinine in the presence of other abundant biomolecules

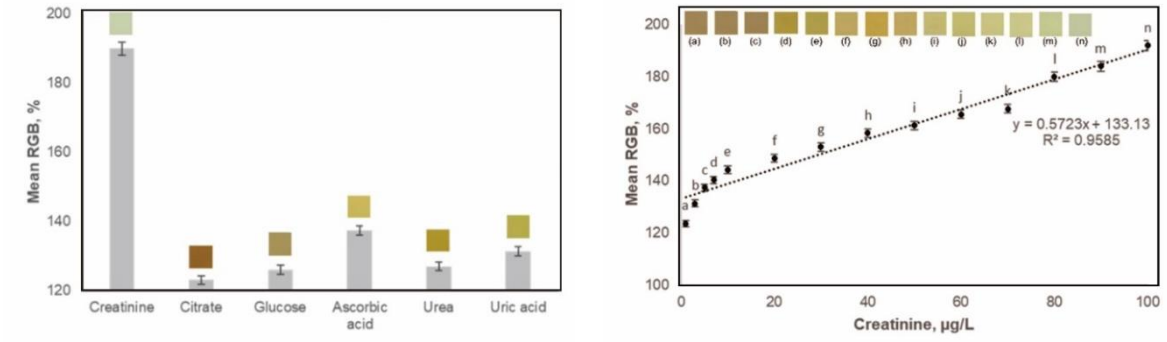

(a) **(b)**

Figure 6. (a) Plot of the mean RGB of AgNP@OAE in the presence of 50 µg/L creatinine or 500 µg/L of interferences; **(b)** the calibration curve of creatinine detection (1 - 100 µg/L). Inset: optical images of the colour change of the sensing probe.

The working performance of the platform was evaluated through calibration studies in the range of 1–100 µg/L creatinine (Figure 6b). A robust linear relationship was established between creatinine concentration and RGB response, as indicated by the regression equation y = 0.5723x + 133.13, with a correlation coefficient (r) of 0.979 and a standard deviation of 0.0129. At a 95% confidence level, with n = 3 and a t-table value (0.05;1) of 6.324, the confidence interval is $0.5249 < \mu < 0.6196$. This high degree of linearity highlights the system's robustness and quantitative capability across a broad concentration domain. The established linear range spans clinically relevant concentrations, confirming that the sensor provides accurate readings for both normal and elevated creatinine levels.

The sensitivity of the method was further defined by calculating the limit of detection (LOD) and the limit of quantification (LOQ). Based on the regression slope and standard deviation (SD) of the blank signal, the LOD and LOQ were determined using equations 1 and 2, giving an LOD value of approximately 1.6 µg/L, while the LOQ was 4.86 µg/L (Table 1).

$$LOD = \frac{3.3 \times SD}{Slope} \quad (1)$$

$$LOQ = \frac{10 \times SD}{Slope} \quad (2)$$

These values demonstrate the method's ability to detect creatinine at very low levels, which is advantageous for early diagnosis and monitoring of renal dysfunction. The relatively low LOD and LOQ reflect the high signal-to-noise performance of the system, further validating its potential for sensitive detection in real-world applications [40].

Reproducibility and repeatability of the assay were examined through replicate analyses at representative concentration levels. The relative standard deviations (RSDs) for intra-day repeatability were less than 4%, while inter-day reproducibility showed RSD values of less than 6% (Table 1). These results indicate excellent precision of the optical readout, with minimal variability between independent measurements. Such reproducible performance ensures that the sensing strategy is reliable and suitable for routine applications, both in laboratory testing and potential point-of-care diagnostics.

Table 1. A comparison of the characteristics of creatinine colorimetric sensors.

Sensing agent	Methods	Linier range (µg/L)	LOD or LOQ (µg/L)	RSD (%)	Ref.
Pectin-Cu/SPCE	Electrochemical sensor	2.3 - 113.12	LOD 1×10^3	3.13	[41]
DNA aptamer–AuNP conjugates	Colorimetry/naked eye detection	226.2 – 2,262.4	LOD 98.41	2.78	[42]
Citrate-AuNPs	Spectrophotometry	0.003 - 0.008	LOD 2.9×10^3	-	[32]
Citrate-AgNPs	Spectrophotometry	0 - 4.7×10^5	LOD 6.0×10^3	-	[19]
Jaffé reagent 3,5-dinitrobenzoate	Colorimetry/RGB Colorimetry/RGB	0 - 2.2×10^6 0 - 2.2×10^6	1.1×10^5 9.2×10^4	<5 <5	[43]
AgNP@OPE	Colorimetry/RGB	1 - 100	LOD 1.6 LOQ 4.86	<4 and <6%	This work

Table 1 provides a comparative overview of various creatinine colorimetric sensors, highlighting their sensing agents, analytical methods, performance ranges, and detection limits. Among the reported systems, electrochemical detection using Pectin-Cu/SPCE exhibits a relatively narrow linear range (2.3–113.12 µg/L) but maintains moderate precision (RSD = 3.13%) [41]. Colorimetric approaches based on DNA aptamer–AuNP conjugates and citrate-stabilized nanoparticles extend the detection window to thousands of µg/L, though their LODs remain higher (98.41 µg/L [42] and 2.9×10^3 µg/L [32], respectively). Traditional Jaffé reagent and 3,5-dinitrobenzoate methods demonstrate broader linear ranges (up to 2.2×10^6 µg/L) [43] but exhibit relatively high limits of detection, indicating limited sensitivity. In contrast, the AgNP@QPE sensor offers a wide linear range (1–100 µg/L) with a low LOD (1.6 µg/L) and LOQ (4.86 µg/L), which is sufficient for clinically relevant creatinine levels. Furthermore, the suggested method has good precision (RSD < 4% at LOD and < 6% overall), comparable or superior to previous colorimetric/RGB-based systems, and allows simple visual or smartphone-assisted detection. Unlike DNA–AuNP aptamers or enzymatic systems, the AgNP@QPE sensor does not require a biorecognition element, thus reducing costs and improving stability. As a result, the primary advantages of this study are not only its sensitivity but also its simplicity, robustness, and versatility for rapid and cost-effective creatinine analysis. These results underline the significant progress in nanoparticle-based sensors, particularly in enhancing analytical sensitivity while simplifying operational requirements for creatinine monitoring.

The practical applicability of the developed assay was evaluated using artificial urine samples spiked with known creatinine concentrations. Before spiking, the samples were diluted with PB buffer (1:20), and the AgNP@OAE-based microfluidic paper assay was conducted at creatinine concentrations of 30 and 80 µg/L. The corresponding recovery results are summarised in Table 2.

Table 2. Recovery of creatinine from spiked artificial urine samples.

Sample	Spiked creatinine (µg/L)	Found creatinine (µg/L)	Recovery (%)	STDEV
S1	30	30.5	101.6	1.55
	30	28.9	96.3	
	30	29.1	97	
S2	80	78.7	98.4	1.81
	80	79.3	99.1	
	80	82.1	102.6	

The applicability of the developed AgNP@OAE-based analytical technology was further tested using spiked artificial urine samples, as shown in Table 2. The method showed good accuracy and precision, with low variability (SD 1.55 - 1.81). All recoveries (96.3–

102.6%) fall within acceptable analytical limits, indicating reliable creatinine determination in spiked artificial urine samples. These findings demonstrate the proposed AgNP@OAE-based microfluidic paper assay's sensitivity and precision in real-sample applications, highlighting its potential for practical diagnostic use in creatinine monitoring.

4. Conclusions

A colorimetric creatinine sensor utilising a biogenic AgNP-based microfluidic paper probe has been successfully developed. Biogenic AgNPs were synthesised using OAE, which is abundant in flavonoid and phenolic compounds (with concentrations of 1.71 and 23.79 mg/g, respectively), as a stabiliser and bioreductant. The AOE solution also serves as an electrolyte in electrosynthesis using Ag electrodes, thereby enabling the development of sensors at affordable costs and environmentally friendly, sustainable synthesis methods. The sensor has a wide linear detection range (1-100 μg/L), a low limit of detection (1.6 μg/L), and high selectivity, repeatability, and reproducibility, making it ideal for point-of-care and resource-limited clinical applications. Future research is required to assess its applicability in clinical samples with more complicated biological matrices and interindividual variability. Long-term sensor storage in changing environments requires further exploration. Despite these challenges, the developed sensor is suitable for routine creatinine monitoring due to its ease of use, low cost, and user- and environmental-friendliness.

Author Contributions

Conceptualization, D.H.; methodology, D.H.; software, B.K.; validation, N.I.; formal analysis, Y.Y. and U.K.Z.; investigation, Y.Y., U.K.Z., and L.K.; resources, B.K.; data curation, N.I.; writing—original draft preparation, D.H.; writing—review and editing, B.K.; visualization, N.I.; project administration, L.K. All authors have read and agreed to the published version of the manuscript.

Institutional Review Board Statement

Not applicable.

Informed Consent Statement

Not applicable.

Data Availability Statement

Data supporting the findings of this study are available upon reasonable request from the corresponding author.

Funding

This research was funded by the University of Mataram, grant number 2451/UN18/L1/PP/2025.

Acknowledgments

The authors sincerely thank the University of Mataram and the University of Jember for invaluable support during the research.

Conflicts of Interest

The authors declare no conflict of interest.

Role of Funders

The funders had no role in the design of the study; in the collection, analyses, or interpretation of data; in the writing of the manuscript, or in the decision to publish the results.

Abbreviations

Abbreviation	Definition
AgNP	Silver Nanoparticle
°C	Degree Celcius
Cm	Centimeter
CKD	Chronic Kidney Disease
DC	Direct Current
DNA	Deoxyribonucleic Acid
EDS	Energy Dispersive Spectroscopy
FCC	Face-Centered Cubic
FWHM	Full Width at Half Maximum
FTIR	Fourier Transform Infra-Red
G	Gram
GCE	Glassy Carbon Electrodes
GFR	Glomerular Filtration Rate
GO	Graphene Oxide
KeV	KiloElectron Volt
L	Liter
LC-IDMS	Liquid Chromatography-Isotope Dilution Mass Spectrometry
LED	Light Emitting Diode
LOD	Limit of Detection
LOQ	Limit of Quantification
LSPR	Localized Surface Plasmon Resonance
mL	Milliliter
MP	Mega-Pixel
µg/L	Microgram per Liter
µPADs	Microfluidic Paper-based Analytical Devices
Mg	Milligram
Nm	Nanometer
OAE	Orthosiphon Aristatus Extract
PB	Phosphate Buffer
PDI	PolyDispersity Index
PSA	Particle Size Analyzer
PSIMS	Paper-Spray Ionization-Mass Spectrometry
PVA	PolyVinyl Alcohol
R	Recovery
RE	Rutin Equivalent
RGB	Red, Green, Blue
RPM	Rotations per Minute
RSD	Relative Standard Deviation
SEM	Scanning Electron Microscopy
SERS	Surface-Enhanced Raman Spectroscopy
TDA	Thio-Diacetic Acid

Abbreviation	Definition
TEM	Transmission Electron Microscopy
TFC	Total Flavonoid Content
TPC	Total Phenolic Content
UV–Vis	Ultraviolet – Visible
V	Volt
XRD	X-Ray Diffraction

References

1. Chapman, C.L.; Johnson, B.D.; Parker, M.D.; Hostler, D.; Pryor, R.R.; Schlader, Z. Kidney physiology and pathophysiology during heat stress and the modification by exercise, dehydration, heat acclimation and aging. *Temperature* **2021**, *8*, 108-159, https://doi.org/10.1080/23328940.2020.1826841.
2. Shlipak, M.G.; Tummalapalli, S.L.; Boulware, L.E.; Grams, M.E.; Ix, J.H.; Jha, V.; Kengne, A.-P.; Madero, M.; Mihaylova, B.; Tangri, N.; Cheung, M.; Jadoul, M.; Winkelmayer, W.C.; Zoungas, S.; Abraham, G.; Ademi, Z.; Alicic, R.Z.; de Boer, I.; Deo, R.; Ding, X.; Ebert, N.; Fowler, K.J.; Fried, L.F.; Gansevoort, R.T.; Garcia-Garcia, G.; Hemmelgarn, B.R.; Lee Harding, J.; Hudson, J.Q.; Iseki, K.; Jotwani, V.; Karliner, L.S.; Levey, A.S.; Liew, A.; Lin, P.J.; Luk, A.O.Y.; Martínez, V.; Moran, A.E.; Nguyen, M.; Obrador, G.T.; O'Donoghue, D.; Pavkov, M.E.; Pavlinac, J.; Powe, N.R.; Seegmiller, J.C.; Shen, J.I.; Shroff, R.; Solá, L.; Taal, M.W.; Tattersall, J.; Vassalotti, J.A.; Weir, M.R.; Zomer, E. The case for early identification and intervention of chronic kidney disease: conclusions from a Kidney Disease: Improving Global Outcomes (KDIGO) Controversies Conference. *Kidney Int.* **2021**, *99*, 34-47, https://doi.org/10.1016/j.kint.2020.10.012.
3. Ávila, M.; Mora Sánchez, M.G.; Bernal Amador, A.S.; Paniagua, R. The Metabolism of Creatinine and Its Usefulness to Evaluate Kidney Function and Body Composition in Clinical Practice. *Biomolecules* **2025**, *15*, 41, https://doi.org/10.3390/biom15010041.
4. Stewart, S.; Kalra, P.A.; Blakeman, T.; Kontopantelis, E.; Cranmer-Gordon, H.; Sinha, S. Chronic kidney disease: detect, diagnose, disclose—a UK primary care perspective of barriers and enablers to effective kidney care. *BMC Med.* **2024**, *22*, 331, https://doi.org/10.1186/s12916-024-03555-0.
5. Kuswandi, B.; Andriani, N.; Nugraha, A.S. Simple monitoring of pH and urea in whole blood using wearable smart woman pad. *BioImpacts* **2022**, *12*, 43–50.
6. Pineda-Cevallos, D.; Funes Menéndez, M.; González-Gago, A.; Rodríguez-González, P.; Ignacio García Alonso, J. Correction of creatine-creatinine conversion during serum creatinine quantification by two-dimensional liquid chromatography and double-spike isotope dilution tandem mass spectrometry. *Clin. Chim. Acta* **2024**, *554*, 117778, https://doi.org/10.1016/j.cca.2024.117778.
7. Sham, T.-T.; Badu-Tawiah, A.K.; McWilliam, S.J.; Maher, S. Assessment of creatinine concentration in whole blood spheroids using paper spray ionization–tandem mass spectrometry. *Sci. Rep.* **2022**, *12*, 14308, https://doi.org/10.1038/s41598-022-18365-8.
8. Atta, S.; Vo-Dinh, T. Improved solution-based SERS detection of creatinine by inducing hydrogen-bonding interaction for effective analyte capture. *Talanta* **2024**, *278*, 126373, https://doi.org/10.1016/j.talanta.2024.126373.
9. Kuswandi, B.; Hidayat, M.A.; Noviana, E. Paper-based sensors for rapid important biomarkers detection. *Biosens. Bioelectron. X* **2022**, *12*, 100246, https://doi.org/10.1016/j.biosx.2022.100246.
10. Narimani, R.; Esmaeili, M.; Rasta, S.H.; Khosroshahi, H.T.; Mobed, A. Trend in creatinine determining methods: Conventional methods to molecular-based methods. *Anal. Sci. Adv.* **2021**, *2*, 308-325, https://doi.org/10.1002/ansa.202000074.
11. Wuyts, B.; Bernard, D.; Van Den Noortgate, N.; Van De Walle, J.; Van Vlem, B.; De Smet, R.; De Geeter, F.; Vanholder, R.; Delanghe, J.R. Reevaluation of Formulas for Predicting Creatinine Clearance in Adults and Children, Using Compensated Creatinine Methods. *Clin. Chem.* **2003**, *49*, 1011-1014, https://doi.org/10.1373/49.6.1011.
12. Ismillayli, N.; Suprapto, S.; Santoso, E.; Nugraha, R.E.; Holilah, H.; Bahruji, H.; Jalil, A.A.; Hermanto, D.; Prasetyoko, D. The role of pH-induced tautomerism of polyvinylpyrrolidone on the size, stability, and antioxidant and antibacterial activities of silver nanoparticles synthesized using microwave radiation. *RSC Adv.* **2024**, *14*, 4509-4517, https://doi.org/10.1039/d3ra07113h.
13. Ismillayli, N.; Suprapto, S.; Jovita, S.; Bahruji, H.; Jalil, A.A.; Hermanto, D.; Prasetyoko, D. The functionalized Ag@SiO_2 core-shell composite for excellent enzyme matrix. *J. Mol. Struct.* **2025**, *1338*,

142308, https://doi.org/10.1016/j.molstruc.2025.142308.
14. Ismillayli, N.; Suprapto, S.; Santoso, E.; Nugraha, R.E.; Holilah, H.; Bahruji, H.; Jalil, A.A.; Hermanto, D.; Prasetyoko, D. Microwave-assisted synthesis of silver nanoparticles as a colorimetric sensor for hydrogen peroxide. *RSC Adv.* **2024**, *14*, 6815-6822, https://doi.org/10.1039/d3ra07775f.
15. Hermanto, D.; Ismillayli, N.; Hamdiani, S.; Kamali, S.R.; Wirawan, R.; Muliasari, H. Paper biosensors utilize silver nanoparticles for onsite pesticide residue detection. *E3S Web Conf.* **2023**, *467*, 01026, https://doi.org/10.1051/e3sconf/202346701026.
16. Hermanto, D.; Ismillayli, N.; Muliasari, H.; Wirawan, R.; Kamali, S.R. Silver-based plasmonic nanoparticles for biosensor organophosphate pesticides using a single film containing acetylcholinesterase/choline oxidase. *Glob. J. Environ. Sci. Manag.* **2024**, *10*, 39–50, https://doi.org/10.22034/gjesm.2024.01.04.
17. Hermanto, D.; Ismillayli, N.; Hamdiani, S.; Kamali, S.R.; Wirawan, R.; Muliasari, H.; Sanjaya, R.K. Inhibitive determination of organophosphate pesticides using acetylcholinesterase and silver nanoparticle as colorimetric probe. *Environ. Eng. Res.* **2024**, *29*, 230503, https://doi.org/10.4491/eer.2023.503.
18. Narimani, R.; Azizi, M.; Esmaeili, M.; Rasta, S.H.; Khosroshahi, H.T. An optimal method for measuring biomarkers: colorimetric optical image processing for determination of creatinine concentration using silver nanoparticles. *3 Biotech* **2020**, *10*, 416, https://doi.org/10.1007/s13205-020-02405-z.
19. Alula, M.T.; Karamchand, L.; Hendricks, N.R.; Blackburn, J.M. Citrate-capped silver nanoparticles as a probe for sensitive and selective colorimetric and spectrophotometric sensing of creatinine in human urine. *Anal. Chim. Acta* **2018**, *1007*, 40-49, https://doi.org/10.1016/j.aca.2017.12.016.
20. Mohammadi, S.; Khayatian, G. Highly selective and sensitive photometric creatinine assay using silver nanoparticles. *Microchim. Acta* **2015**, *182*, 1379–1386, https://doi.org/10.1007/s00604-015-1460-5.
21. Khursheed, S.; Sarwar, S.; Hussain, D.; Shah, M.R.; Barek, J.; Malik, M.I. Electrochemical detection of creatinine at picomolar scale with an extended linear dynamic range in human body fluids for diagnosis of kidney dysfunction. *Anal. Chim. Acta* **2025**, *1353*, 343978, https://doi.org/10.1016/j.aca.2025.343978.
22. Batubara, I.; Komariah, K.; Sandrawati, A.; Nurcholis, W. Genotype selection for phytochemical content and pharmacological activities in ethanol extracts of fifteen types of *Orthosiphon aristatus* (Blume) Miq. leaves using chemometric analysis. *Sci. Rep.* **2020**, *10*, 20945, https://doi.org/10.1038/s41598-020-77991-2.
23. Hermanto, D.; Ismillayli, N.; Wiranatasari, T.A.L.; Mudasir; Siswanta, D.; Kuswandi, B.; Siswoyo; Suprapto; Prasetyoko, D. Electrosynthesis of Anisotropic Biogenic Silver Nanoparticles as a Promising Antibacterial Agent using *Stachytarpheta jamaicensis* Leaf Extract. *Sains Malaysiana* **2024**, *53*, 3113-3123, https://doi.org/10.17576/jsm-2024-5309-16.
24. Hermanto, D.; Ismillayli, N.; Irmawanti, I.; Fathulloh, I.; Nila, D.; Zuryati, U.K.; Muliasari, H.; Wirawan, R. Electrochemically synthesized biogenic silver nanoparticles using green tea extract as a promising antioxidant. *Karbala Int. J. Mod. Sci.* **2023**, *9*, 8, https://doi.org/10.33640/2405-609X.3276.
25. Sarigul, N.; Korkmaz, F.; Kurultak, I. A New Artificial Urine Protocol to Better Imitate Human Urine. *Sci. Rep.* **2019**, *9*, 20159, https://doi.org/10.1038/s41598-019-56693-4.
26. Khaydarov, R.A.; Khaydarov, R.R.; Gapurova, O.; Estrin, Y.; Scheper, T. Electrochemical method for the synthesis of silver nanoparticles. *J. Nanoparticle Res.* **2009**, *11*, 1193-1200, https://doi.org/10.1007/s11051-008-9513-x.
27. Waldvogel, S.R.; Mentizi, S.; Kirste, A. Boron-Doped Diamond Electrodes for Electroorganic Chemistry. In Radicals in Synthesis III; Heinrich, M., Gansäuer, A., Eds.; Springer Berlin Heidelberg: Berlin, Heidelberg, **2012**; Volume 320, pp. 1-31, https://doi.org/10.1007/128_2011_125.
28. Hoang, V.-T.; Dinh, N.X.; Pham, T.N.; Hoang, T.V.; Tuan, P.A.; Huy, T.Q.; Le, A.-T. Scalable Electrochemical Synthesis of Novel Biogenic Silver Nanoparticles and Its Application to High-Sensitive Detection of 4-Nitrophenol in Aqueous System. *Adv. Polym. Technol.* **2021**, *2021*, 6646219, https://doi.org/10.1155/2021/6646219.
29. Hussain, S.; Khan, Z. Epigallocatechin-3-gallate-capped Ag nanoparticles: preparation and characterization. *Bioprocess Biosyst. Eng.* **2014**, *37*, 1221–1231, https://doi.org/10.1007/s00449-013-1094-0.
30. Bhandari, S.; Parihar, V.S.; Kellomäki, M.; Mahato, M. Highly selective and flexible silver nanoparticles-based paper sensor for on-site colorimetric detection of paraquat pesticide. *RSC Adv.* **2024**, *14*, 28844-28853, https://doi.org/10.1039/d4ra04557b.
31. Gomeceria, M.A.D.; Miranda, M.L.I.C.; Lopez, E.C.R.; Perez, J.V.D. Fabrication of Paper-Based Silver

Nanoparticle (AgNP) Sensors for Smartphone-Based Colorimetric Detection of Cu (II) in Water. *Mater. Sci. Forum* **2024**, *1112*, 109-117, https://doi.org/10.4028/p-VYbuw7.
32. He, Y.; Zhang, X.; Yu, H. Gold nanoparticles-based colorimetric and visual creatinine assay. *Microchim. Acta* **2015**, *182*, 2037–2043, https://doi.org/10.1007/s00604-015-1546-0.
33. Jayeoye, T.J; Ma, J.; Rujiralai, T. Creatinine assembled on dithiobis(succinimidylpropionate) modified gold nanoparticles as a sensitive and selective colorimetric nanoprobe for silver ion detection. *J. Environ. Chem. Eng.* **2021**, *9*, 105770, https://doi.org/10.1016/j.jece.2021.105770.
34. He, Y.; Liang, Y.; Song, H. One-pot Preparation of Creatinine-functionalized Gold Nanoparticles for Colorimetric Detection of Silver Ions. *Plasmonics* **2016**, *11*, 587–591, https://doi.org/10.1007/s11468-015-0092-2.
35. Huang, J.; Sokolikova, M.; Ruiz-Gonzalez, A.; Kong, Y.; Wang, Y.; Liu, Y.; Xu, L.; Wang, M.; Mattevi, C.; Davenport, A.; Lee, T.-C.; Li, B. Ultrasensitive colorimetric detection of creatinine *via* its dual binding affinity for silver nanoparticles and silver ions. *RSC Adv.* **2024**, *14*, 9114-9121, https://doi.org/10.1039/d3ra08736k.
36. Patle, T.K.; Shrivas, K.; Kurrey, R.; Upadhyay, S.; Jangde, R.; Chauhan, R. Phytochemical screening and determination of phenolics and flavonoids in *Dillenia pentagyna* using UV–vis and FTIR spectroscopy. *Spectrochim. Acta A Mol. Biomol. Spectrosc.* **2020**, *242*, 118717, https://doi.org/10.1016/j.saa.2020.118717.
37. Hermanto, D.; Ismillayli, N.; Fatwa, D.H.; Zuryati, U.K.; Muliasari, H.; Wirawan, R.; Prasetyoko, D.; Suprapto, S. Bio-mediated electrochemically synthesis of silver nanoparticles using green tea (Camellia sinensis) leaves extract and their antibacterial activity. *S. Afr. J. Chem. Eng.* **2024**, *47*, 136-141, https://doi.org/10.1016/j.sajce.2023.11.004.
38. Salih, H.H. Biosynthesis of Silver Nanoparticles by Using Green Tea (Camellia sinensis) Extracts. *Baghdad Sci. J.* **2024**, *21*, 1470, https://doi.org/10.21123/BSJ.2023.8344.
39. Shareef, A.A.; Farhan, F.J.; Alriyahee, F.A.A. Green Synthesis of Silver Nanoparticles Using Aqueous Extract of Typha domingensis Pers. Pollen (qurraid) and Evaluate its Antibacterial Activity. *Baghdad Sci. J.* **2024**, *21*, 5, https://doi.org/10.21123/bsj.2023.7624.
40. Krissanjaya, R.; Hermanto, D.; Ismillayli, N.; Savitri, L.; Probojati, R.T.; Masyhuri, A.A.; Sianturi, J. High-performance urease-BTB/silicalite optical biosensor for real-time urea detection. *Microchem. J.* **2026**, *220*, 116324, https://doi.org/10.1016/j.microc.2025.116324.
41. Hou, H.; Li, F.; Lin, S.; Li, Z.; Li, X. Non-invasive detection of urinary creatinine levels using a non-enzymatic electrochemical sensor with pectin-assisted Cu electrodeposition. *Microchem. J.* **2025**, *209*, 112783, https://doi.org/10.1016/j.microc.2025.112783.
42. Das, C.; Raveendran, J.; Bayry, J.; Rasheed, P.A. Selective and naked eye colorimetric detection of creatinine through aptamer-based target-induced passivation of gold nanoparticles. *RSC Adv.* **2024**, *14*, 33784–33793, https://doi.org/10.1039/d4ra06191h.
43. Lewińska, I.; Speichert, M.; Granica, M.; Tymecki, Ł. Colorimetric point-of-care paper-based sensors for urinary creatinine with smartphone readout. *Sensors Actuators B: Chem.* **2021**, *340*, 129915, https://doi.org/10.1016/j.snb.2021.129915.

Publisher's Note & Disclaimer

The statements, opinions, and data presented in this publication are solely those of the individual author(s) and contributor(s) and do not necessarily reflect the views of the publisher and/or the editor(s). The publisher and/or the editor(s) disclaim any responsibility for the accuracy, completeness, or reliability of the content. Neither the publisher nor the editor(s) assume any legal liability for any errors, omissions, or consequences arising from the use of the information presented in this publication. Furthermore, the publisher and/or the editor(s) disclaim any liability for any injury, damage, or loss to persons or property that may result from the use of any ideas, methods, instructions, or products mentioned in the content. Readers are encouraged to independently verify any information before relying on it, and the publisher assumes no responsibility for any consequences arising from the use of materials contained in this publication.